Pharm Res (2013) 30:2538–2548
DOI 10.1007/s11095-013-1004-9

RESEARCH PAPER

Up-regulating Blood Brain Barrier Permeability of Nanoparticles *via* Multivalent Effect

Xihui Gao • Jun Qian • Shuyan Zheng • Ying Xiong • Jiahao Man • Binxin Cao • Lu Wang • Shenghong Ju • Cong Li

Received: 14 September 2012 / Accepted: 6 February 2013 / Published online: 15 March 2013

ABSTRACT

Purpose To investigate the multivalent effect for up-regulating the intracerebral delivery of nanoparticles *via* receptor-mediated transcytosis.

Methods Nanoparticles labeled with near-infrared (NIR) fluorophore and different numbers of angiopep-2 peptides that specifically target low-density lipoprotein receptor-related protein (LRP) on the brain capillary endothelial cells were developed. Bio-distribution studies quantified the intracerebral uptakes of these nanoparticles at 2 and 24 h after intravenous injection. *In vivo* NIR fluorescence imaging, *ex vivo* autoradiographic imaging and 3D reconstructed NIR fluorescence imaging revealed the nanoparticle distribution pattern in brain. Fluorescence microscopic imaging identified the nanoparticle locations at the cellular level.

Results The multimetirc association between the angiopep-2 peptides labeled on the nanoparticle and the LRP receptors on the brain capillary endothelial cells significantly increased the intracerebral uptake of the nanoparticles. Nanoparticle Den-Angio4 labeled four angiopep-2 peptides achieved the highest BBB traverse efficacy. After penetrating the BBB, Den-Angio4 distributed heterogeneously and mainly located at hippocampus, striatum and cerebellum in the brains.

Conclusions The multivalent effect significantly enhances the BBB permeability of nanoparticles. Den-Angio4 as a nanoparticle prototype provides a two order targeted strategy for diagnosis or treatment of central nerver system diseases by first traversing the BBB *via* receptor-mediated endocytosis and secondly targeting the leisions with high receptor expression level.

KEY WORDS blood brain barrier · LRP receptor · multivalent effect · nanoparticle · receptor-mediated endocytosis

ABBREVIATIONS

BBB	Blood brain barrier
BCEC	Brain capillary endothelial cells
CNS	Central nervous system
DiO	3,3′-dioctadecyloxacarbocyanine perchlorate
LRP	Low-density lipoprotein receptor-related protein
NIR	Near-infrared
PFA	Paraformaldehyde
PI	Post-injection
SDS-PAGE	Sodium dodecyl sulfate-polyacrylamide gel electrophoresis

INTRODUCTION

Blood brain barrier (BBB) is a physiological structure that restricts the movement of molecules and cells between blood and brain, provides a natural defense against circulating toxic or infectious substances, and maintains the ions and fluid balance to ensure an optimal environment for brain function (1). Due to the low permeability of BBB, more than 98% small molecular and almost all macromolecular drugs can not be delivered into brain (2), which is a nightmare for the diagnosis and therapy of central nervous system (CNS) related diseases. Receptor-mediated endocytosis is a natural

Electronic supplementary material The online version of this article (doi:10.1007/s11095-013-1004-9) contains supplementary material, which is available to authorized users.

X. Gao • J. Qian • S. Zheng • Y. Xiong • J. Man • B. Cao • L. Wang • C. Li (✉)
Key Laboratory of Smart Drug Delivery, Ministry of Education & PLA School of Pharmacy, Fudan University, Shanghai 201203, China
e-mail: congli@fudan.edu.cn

S. Ju (✉)
Jiangsu Key Laboratory of Molecular and Functional Imaging Department of Radiology, Zhongda Hospital, Medical School Southeast University, Nanjing 210009, China
e-mail: jsh0836@hotmail.com

pathway through which endogeneous proteins traverse the BBB and this approach is recognized by the scientific community as a promising strategy for intracerebral drug delivery (3,4). For example, transferrin (Tf), the ligand of Tf receptor has been functionalized into drug-delivery vectors to transport small molecular drugs (5), proteins (6), and gene materials (7) into brain (8). Similar to Tf receptor, nicotinic acetylcholine receptor (nAChR) (9), low-density lipoprotein receptor-related protein (LRP) (10) and $GABA_B$ receptor (11) that present on the brain capillary endothelial cells (BCECs) also show the capacity for intracerebral transport of their corresponding ligands. Therefore, ligands such as lectoferrin (Lf) (12), rabies virus glycoprotein peptide (RVG29) (11), snake neurotoxin candoxin peptide (CDX) (9) and angiopep-2 peptide were conjugated to the drug delivery vectors to up-regulate their BBB permeability. Angiopep-2, a 19 amino acid peptide derived from Kunitz domains of aprotinin, demonstrates a higher BBB transcytosis capacity than Tf and its parent molecule aprotinin (10). Importantly, LRP receptors not only present in BCECs, but also express in many types of brain cancer cells (13) as well as neurons with up-regulated Aβ peptide that is known as a component of amyloid plaques in association with Alzheimer's disease (14,15). Therefore, vectors modified with angiopep-2 peptide can specifically deliver the drugs to CNS related diseases by first penetrating BBB *via* LRP receptor-mediated endocytosis followed targeting to the lesions with high expression level of LRP receptors.

Multivalent interaction, the simultaneous binding event of multiple ligands to multiple receptors in biological systems, has been investigated to dramatically enhance targeting specificity of drug delivery/imaging agents. Liu *et al.* reported a series of radiolabled multimeric cyclic RGD peptides to image tumor by targeting the $\alpha_V\beta_3$ integrin over-expressed in tumor neovasculatures as well as cancer cells (16). The binding affinity of the radiotracers to $\alpha_V\beta_3$ integrin increased with the multimetric degree. For example, the IC_{50} value of the tetrameric cyclic c[RGDyK] peptide was determined as 106 times lower than that of monomeric c[RGDyK] peptide (17). Compared to small molecules, nanoparticles are more promising to achieve multivalent effect because of the convenience to label multiple copies of ligands on the particle surface. Meanwhile, the tunable circulation lifetime (18,19) and the flexibility for conformational deformation (20) of the nanoparticles further increase their binding affinity to the targeted receptor. For example, Baker *et al.* prepared a series of G5 dendrimer-based nanoparticles functionalized with multiple copies of folic acids (21). The normalized binding affinity per folic acid in the nanoparticle was determined as 15,200 times higher compared to that of free folic acid. Even the multivalent effect of nanoparticles has been successfully applied in tumor imaging and therapy, as far as we known, the role it played in influencing the brain uptake of nanoparticles has not been investigated. As shown in Fig. 1, we suspect the multimetric association between the peptides labeled on the nanoparticles and receptors on the BCECs can increase the local concentration of nanoparticle on the brain capillaries and hence accelerate the receptor-mediated endocytosis.

Optical imaging as a developing imaging modality demonstrates superior sensitivity (pM−nM), fast-acquisition time (ms−s) and no radioactive irradiation (22). Fluorescence probes that excite and emit in a near-infrared (NIR) wavelength range (650–900 nm) show advantages for *in vivo* imaging because the absorbance and autofluorescence from endogenous molecules are low, which benefits to visualize biological events with high sensitivity and spatial resolution in deep tissues (23). Our previous work also confirmed that the NIR fluorescence can penetrate the mouse skull and visualize the orthotropic brain tumor non-invasively *in vivo* (13,24). In this work, nanoparticles labeled with NIR fluorophore and multiple copies of BBB permeable angiopep-2 peptides were developed. As far

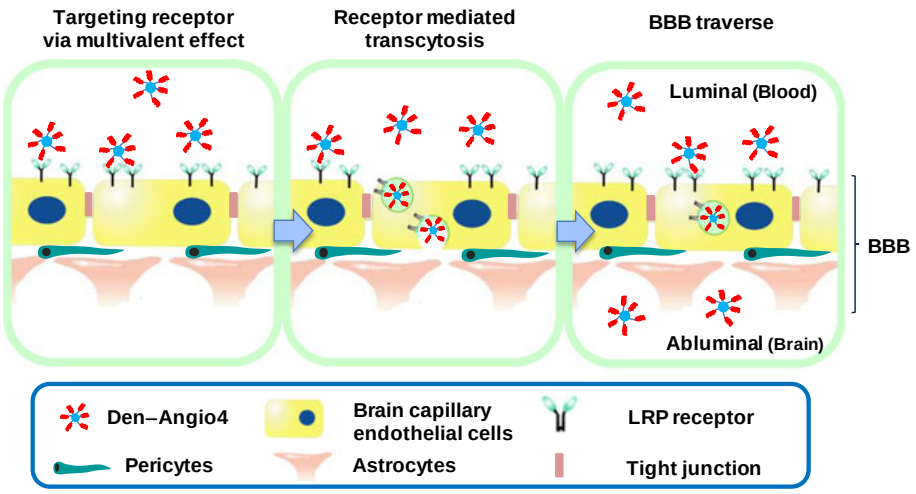

Fig. 1 Overview of multivalent effect accelerating BBB permeability of the angiopep-2 labeled nanoparticle. Multimetric association between the nanoparticles and LRP receptors increases the local concentration of nanoparticles on the brain capiliaries and hence enhances the BBB traverse efficacy *via* LRP receptor-mediated endocytosis.

as we know, this is the first time to systemically investigate the role of multivalent effect played in enhancing BBB permeability of nanoparticle by a non-invasive optical imaging strategy.

MATERIALS AND METHODS

Materials

PAMAM G5 dendrimer was purchased from Dendritech Inc (Midland, MI, USA). Rhodamine N-hydroxysuccinimidyl (NHS) ester and *N*-succinimidyl 3-(2-pyridyldithio) propionate (SPDP) were purchased from Invitrogen (Carlsbad, CA, USA). Activated polyethylene glycol derivatives PEG^{2k}-NHS ester and NH_2-PEG^{2k}-Malemide were purchased from JenKem Technology Co. Ltd (Beijing, China). IR783-NHS ester was prepared at home according to our previous report (25). Amicon ultra-15 centrifugal filter tubes (10,000 MW cut off) were purchased from Millipore (Bedford, MA, USA). All organic solvents were analytical grade from Aladdin Reagent (Shanghai, China) unless otherwise specified. Male ICR mice, aging 4–5 weeks and weighing 20±2 g, supplied by Department of Experimental Animals, Fudan University (Shanghai, China) were acclimated at 25°C and 55% humidity under natural light/dark conditions for 1 week before experiment. All animal experiments were carried out in accordance with guidelines evaluated and approved by the ethics committee of Fudan University (Shanghai, China).

Synthesis

Angiopep-2 Peptide

TFFYGGSRGKRNNFKTEEYC (MW=2,402 Da) with a cysteine residue labeled at C' terminal of the angiopep-2 peptide was synthesized *via* Boc-protected solid-phase peptide synthesis strategy. The obtained fully protected linear peptide H-Thr(Bzl)-Phe-Phe-Tyr(Br-Z)-Gly-Gly-Ser(Bzl)-Arg(Tos)-Gly-Lys(Cl-Z)-Arg(Tos)-Asn(Xan)-Asn(Xan)-Phe-Lys(Cl-Z)-Thr(Bzl)-Glu(OcHex)-Glu(OcHex)-Tyr(Br-Z)-Cys(PMeBzl)-OH was deprotected in hydrofluoric acid (HF) and purified by preparative HPLC followed lyophilization. The purity was verified by analytic HPLC. The mass was 802.5 [M^{3+}] (calculated 2404.6 [M + H^+]) as determined by Electron Spray Ionization (ESI) mass spectrometer.

Control Nanoparticle Den-PEG

PEG^{2K}-NHS ester (14 mg, 7×10^{-6}mol) dissolved in 50 μL anhydrous DMF was added dropwise into 1.0 mL 0.1 M HEPES buffered solution (pH8.5) of G5 dendrimer (11.6 mg, 4.0×10^{-7}mol). After stirring at 25°C for 2 h, the mixture was purified by a centrifuge in a centrifugal filter (MW 10,000 cut off) to obtain compound **1**. To a solution of **1** in 1.0 mL 0.1 M HEPES buffered solution (pH8.5), Rhodamine-NHS ester (0.4 mg, 8.0×10^{-7}mol) in 50 μL anhydrous DMF and IR783-NHS ester (0.78 mg, 8.0×10^{-7}mol) in 50 μL anhydrous DMF were added dropwise. After stirring at 25°C for 1.0 h, the dual-fluorophore conjugated dendrimer was purified and desiccated under vacuum to offer the nanoparticle Den-PEG as a purple powder (3.20×10^{-7}mol, yield: 80%).

BBB Permeable Nanoparticles Den-Angio1, Den-Angio4 and Den-Angio8

N-succinimidyl 3-(2-pyridyldithio) propionate (SPDP) (2.9 mg, 9×10^{-6}mol) in 300 μL DMF was added into the 1.0 mL PBS solution (pH7.4) of NH2-PEG^{2k}-Mal (14 mg, 7×10^{-6}mol) and reacted at 25°C for 1.0 h. Without purification, the resulting compound **2** with maleimide and SPDP modified at its two terminals was added into G5 dendrimer (11.6 mg, 4.0×10^{-7}mol) in 1.0 mL HEPES buffered solution (0.1 M, pH8.5). After stirring at 25°C for 2 h, the mixture was purified by centrifuge to remove the by-products and obtain compound **3**. Rhodamine-NHS ester IR783-NHS ester (0.4 mg, 8.0×10^{-7}mol) and IR783-NHS ester (0.78 mg, 8.0×10^{-7}mol) were labelled into compound **3** (15.2 mg, 3.12×10^{-7}mol) respectively as described above to obtain the compound **4**. To three potions of compound **4** (19.5 mg, 4.0×10^{-7}mol) in 2.0 mL PBS, cysteine labelled angiopep-2 peptide (2.08 mg, 8.5×10^{-7}mol; 8.40 mg, 3.5×10^{-6}mol; 14.6 mg, 6.1×10^{-6}mol) in 200 μL DMF was added respectively. After stirring at 25°C for overnight and purifying in the centrifugal filter, the aiming nanoparticles Den-Angio1, Den-Angio4, Den-Angio8 were obtained with yields in a range of 72–81%.

Characterization

The Composition of Nanoparticles

The molar ratios between G5 dendrimer, PEG, and angiopep-2 peptide in the nanoparticles were quantified by ^{1}H NMR (Varian Mercury400 spectrometer, USA). The molar ratios of the main components in the nanoparticles were determined by integrating the characteristic proton of dendrimer, PEG and angiopep-2 in the ^{1}H NMR spectra.

The Purity of Nanoparticles

The nanoparticle purities were determined by sodium dodecyl sulfate-polyacrylamide gel electrophoresis (SDS-

PAGE). Nanoparticle (50 μg) in 30 μL treatment buffer [100 mM Tris, pH6.8, 2% (w/v) SDS, 12% (v/v) glycerol, 0.01% (w/v) bromphenol blue] was loaded on a 10% polyacrylamide gel. After electrophoresis under a voltage of 70 V for 2 h, white light and fluorescent images of the resolved SDS-PAGE gels were collected on a Maestro™ *In Vivo* Multispectral Imaging System. The IR783 fluorescence was collected by using the NIR filter set (710–760 nm excitation filter and 800 nm emission filter, exposure time: 800 ms); the Rhodamine fluorescence was obtained by using the Blue filter set (503–555 nm excitation filter and 580 nm emission filter, exposure time: 200 ms).

Hydrodynamic Size Distribution and Zeta Potentials of the Nanoparticles

Hydrodynamic radius of nanoparticles were measured by dynamic light scattering (DLS) using a Malvern Zetasizer ZS instrument (Malvern Instruments Ltd, UK). The working solutions of the nanoparticles (100 μg/mL in PBS) were filterated through 0.45 μm filter before the measurement. Bovine serum albumin (BSA, 2.0 mg/mL) in distilled water was used as a standard for the instrument calibration. To measure the surface charges of the nanoparticles, the instrument was calibrated with the standard solution with a Zeta potential of −50 mV. The nanoparticles (200 μg/mL) in 10 mM NaCl solution were sterilized by filtrating through a 0.45 μm filter prior to the measurement.

Cell Culture and Flow Cytometry Studies

Human glioblastoma U87MG cells were grown as monolayers in 75-cm^2 flasks containing Minimum Essential Medium, Alpha 1X (MEM, Mediatech, Manassas, VA) supplemented with 10% fetal bovine serum (FBS), 2 mM L-glutamine, 1% penicillin and streptomycin (Invitrogen, Carlsbad, CA) in a fully-humidified incubator containing 5% CO_2 at 37°C. Cells with 80% confluence were treated with 1.0 μM nanoprobe in which the rhodamine was replaced by fluorescein at 4°C for 30 min. At the end of incubation, the cells were washed 3X by PBS, centrifuged, fixed in 0.5% PFA, and analyzed by BD FACSAria (BD Biosciences, USA) equipped with a 488 nm Ar ion laser

Bio-distribution

Radiolabeling of Nanoparticle with Radioactive ^{125}Iodide (^{125}I)

Nanoparticles were radiolabeled with ^{125}I isotope on the primary amines of dendrimer by using Bolton-Hunter reagent (Pierce Biotechnology, USA) (26). Briefly, appropriate amount of Bolton-Hunter reagent, 1.0 mCi of $Na^{125}I$ and Chloramine-T were mixed and oscillated for 10 s. Then, sodium pyrosulfite and NaI in PB solution, DMF and benzene were added sequently. The organic layer was separated and evaportaed to obtain the radiolabeled Bolton-Hunter reagent. After reaction with nanoparticles in PBS at 25°C for 1.0 h, the ^{125}I labeled nanoparticles were obtained after purification by centrifuge.

Animal Experiment

Forty healthy mice (18–22 g) were randomly divided into eight groups and each group was injected intravenously with corresponding [^{125}I]-labeled nanoparticle (3.7×10^5 Bq/mouse). The animals were anesthetized at 2 and 24 h post-injection (PI), perfused with saline and the tissues of interest (blood, whole brain, heart, spleen, lung, liver, kidney and muscle) were harvested, weighed, and the radioactivities were counted with an SN-695 intelligent γ-counter (Shanghai Hesuo Rihuan Photoelectric Instrument CO Ltd, China). After the measurement, selected components of brains including cerebral cortex, hippocampus, striatum, cerebellum and the left cerebral tissues were carefully separated, weighed, and counted. The uptakes were calculated as a percentage of the injected dose per gram of organ tissue (%ID/g). The biodistribution data were reported as an average plus the standard deviations from at least four mice at each time point.

Autoradiographic Imaging

Mice brains at 2 or 24 h post-injection of ^{125}I radiolabeled nanoparticles (3.7×10^5Bq/mouse) were excised, prefixed and sectioned coronally with a thickness of 1.0 mm. The brain sections were mounted on a transparent wrap in sequence and exposed to a phosphor storage screen film (super-resolution screen; Perkin Elmer) for 10 h. Read of the screens by a Cyclone Pulse Storage Phosphor system (Perkin-Elmer, USA) offered the autoradiography images, which were further analyzed by using an Optiquant software (Perkin Elmer). Meanwhile, the white light images of these brain sections were taken by a Leica MZ75 high performance stereomicroscope (Leica Inc., Germany) equipped with 2.5X objective lens.

In Vivo and *Ex Vivo* Optical Imaging

NIR fluorescence images of the mouse brain area were acquired at selected time-points after systemic injection of nanoparticle (5.0 nmol based on dendrimer) with a same exposure time of 2.0 s. At the end of *in vivo* imaging, the mice were perfused with saline and 4% paraformaldehyde (PFA) in succession *via* heart to douche blood and pre-fix the mouse. Brains were carefully isolated and the NIR fluorescence images of whole brains were captured with an

exposure time of 2.0 s. The average fluorescence intensity was calculated by using ImageJ software.

3D Reconstructed NIR Fluorescence Image

At selected time PI of nanoparticle, the mice were scarified, perfused with saline followed lipophilic carbocyanine dye DiO to stain the vasculatures, and then pre-fixed with PFA. The excised brains were put into a stainless mouse brain matrix (Beijing Sunny Instruments Co. Ltd., China) and sectioned coronally with a thickness of 1.0 mm. These brain sections were tiled horizontally on a glass slide and imaged. The rhodamine fluorescence that indicates the nanoparticle position and DiO fluorescence that indicates the vasculatures were acquired for each of the brain sections. To straightforwardly visualize the nanoparticle distribution in brain, fluorescence images of brain sections were converted into gray format, modified with a same size and reconstructed by Amira 5.2.1 software (Visage Imaging Inc.).

Fluorescence Microscopic Imaging

The isolated brains were immersed in 4% PFA for 12 h, 30% sucrose solution for 24 h and sectioned coronally with a thickness of 5.0 μm. The fluorescence microscopic images were collected in Leica DMF4000B laser-scanning microscope (Leica Inc, Wetzlar, Germany) equipped with a 10X objective len. The DAPI fluorescence was collected by using an A4 filter tube (excitation: 360±20 nm and emission: 470 ±20 nm), the DIO fluorescence was obtained by using a L5 filter (excitation: 480±20 nm and emission: 527±15 nm) and the rhodamine fluorescence was obtained by using a N3 filter (excitation: 546±6 nm and emission: 600±20 nm). All the microscopic images were captured with an identical microscopic setting. The fluorescence intensities were quantified by ImageJ (NIH, Bethesda, MD) software.

Statistical Analysis

All data are presented as mean ± SD (standard deviation) of at least three experiments. We analyzed statistical differences by Student's *t* test (Microsoft Excel 2002, Microsoft Corp, WA). Statistical significance was defined at the level of $P<0.05$ (two-tailed).

RESULTS AND DISCUSSION

Design, Synthesis, and Characterization of the Nanoparticles

The fifth generation (G5) PAMAM dendrimer was chosen as a platform of the nanoparticles due to its globular architecture, identical molecular weight, optimized circulation lifetime, and well-defined reactive groups on the particle surface (18). IR783 was chosen as NIR fluorophores here because of its high extinction coefficient, optimal emission wavelength and good photophysical stability (27,28). Rhodamine was used to track the nanoparticles in either cells or excised tissues because NIR fluorophore IR783 cannot be excited well under a conventional fluorescent microscope. Angiopep-2 peptides were labeled on the dendrimer through a PEG linker. The extended PEG linker not only improves the biocompatibility of the nanoparticle but also minimizes the steric hindrance of the hyperbranched polymer to the targeting specificity of ligands (24).

To clarify the role multivalent effect played in up-regulating the brain uptake, nanoparticles Den-Angio1, Den-Angio4 and Den-Angio8 that labeled with different numbers of angiopep-2 peptides and the control nanoparticle Den-PEG without any peptide were developed. Briefly, treatment of G5 dendrimer (29 kDa) with NHS esters of PEG^{2k} in 0.1 M HEPES (pH8.3) gave compound **1**. Reaction of **1** with NHS esters of rhodamine and IR783 respectively offered the control nanoparticle Den-PEG (Fig. 2a). The general synthetic procedure to prepare the BBB permeable nanoparticles was indicated in Fig. 2b. Treatment of bis-functionalized PEG derivative Mal-PEG^{2k}-NH_2 with N-succinimidyl 3-(2-pyridyldithio) propionate (SPDP) offered compound **2**, which further reacted with G5 dendrimer to give **3** that were averagely labeled nine PEG derivatives respectively. The conjugation of **3** with NHS esters of rhodamine and IR783 gave **4**, which then reacted with different amount of cysteine modified angiopep-2 peptide to offer aiming nanoparticles Den-AngioX (X=1, 4, 8). To clarify the role of multivalent effect played in up-regulating the BBB permeability, the nanoparticle should have identical chemical structure except the number of the conjugated angiopep-2 peptides. To achieve this goal, compound **4** modified with averagely nine reactive PEG linkers was synthesized first and then treated with selected amount of angiopep2 peptides. Our experimental data further indicated that averagely two molar equivalents of cysteine modified angiopep-2 peptides can label one of the PEG moiety on the nanoparticle. By this way, the number of conjugated peptides on the nanoparticles can be finely adjusted. The purity of the nanoparticles was tested by the white light and fluorescence images of the resolved sodium dodecyl sulfate-polyacrylamide gel electrophoresis (SDS-PAGE) (Fig. 2c). All the nanoparticles migrated as a single band that verified their low polydispersity after multiple modifications. Notably, the migration distances of the nanoparticles decreased with a sequence of Den-PEG > Den-Angio1 > Den-Angio4 > Den-Angio8, which correlated well with the increase of their molecular weights. Furthermore, the bands of the nanoparticles in the

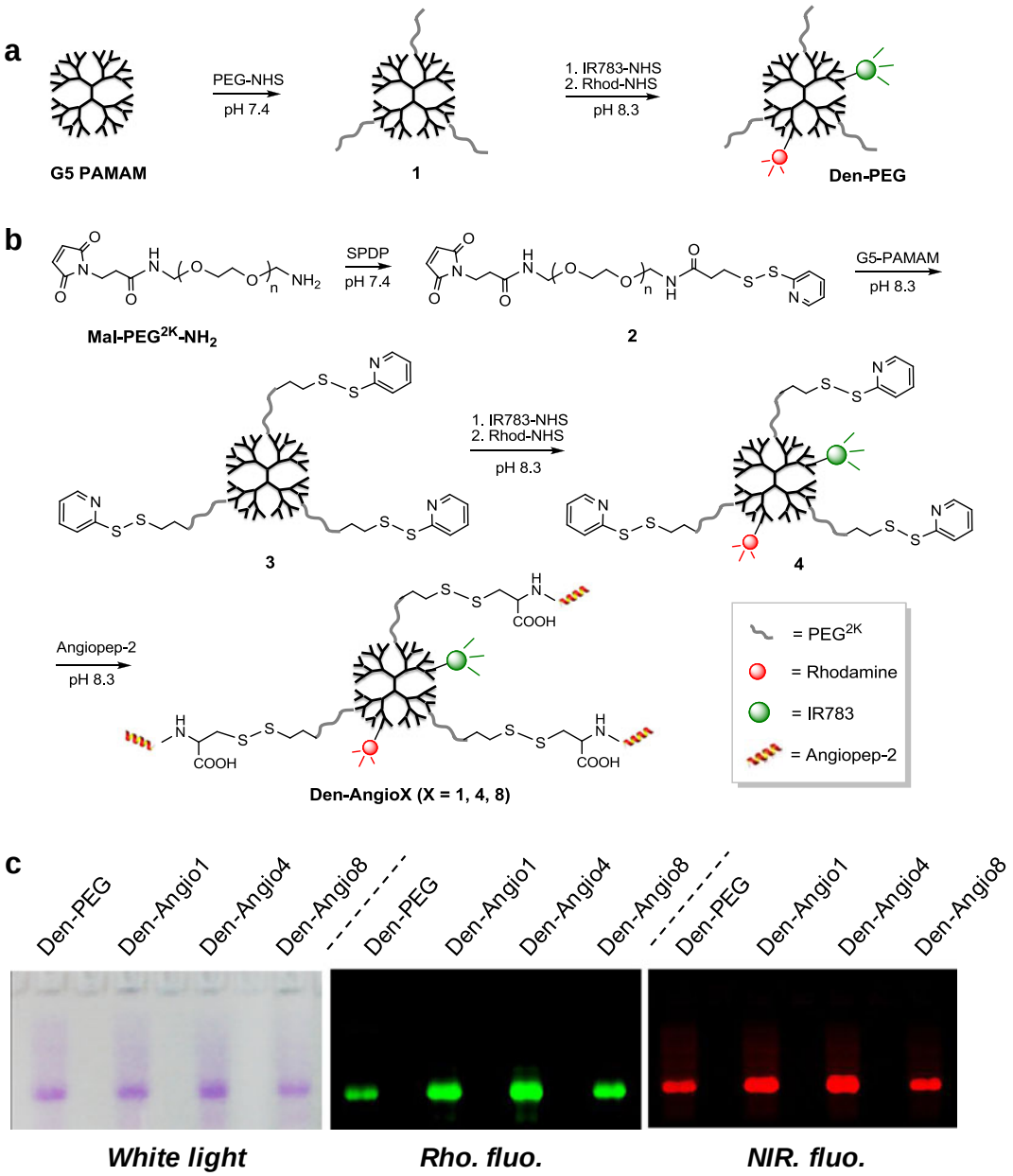

Fig. 2 Synthesis of the control nanoparticle (**a**) and the BBB permeable nanoparticles (**b**). **c** White light and fluorescence images of the resolved SDS-PAGE after loading 50 μg nanoparticles. The migration bands of nanoparticles in the rhodamine and NIR fluorescence images were displayed in green and red respectively.

rhodamine fluorescence image and NIR fluorescence image fully colocalize with each other. Above data verified the conjugation of these two types of fluorophores on the nanoparticle.

The physical parameters and the molar ratioes between the functional groups and dendrimer in the nanoparticles were listed in Table I. Notably, the hydrodynamic diameters of the nanoparticles increased slightly with the labeling degree of the angiopep-2 peptides. Interestingly, even each angiopep-2 peptide possesses two positive net charges under neutral pH, the surface charges of the nanoparticles barely changed with the labeling degree of the peptides. The water

Table I Physical Parameters of the Nanoparticles

Nanoprobe	d (nm)[a]	PDI[a]	ξ[a]	Den/PEG/Angio[b]
Den-PEG	6.9	0.259	+5.4	1/8.9/0
Den-Angio1	7.2	0.314	+6.1	1/8.2/1.2
Den-Angio4	7.4	0.345	+6.4	1/8.2/4.2
Den-Angio8	7.9	0.269	+7.2	1/8.2/8.1

[a] Diameters (*d*), polydispersity index (*PDI*), and zeta potentials (ζ) were measured by dynamic light scattering (*DLS*)

[b] Molar ratioes of Den/PEG/Angiopep-2 in the nanoparticles were determined by ^{1}H NMR

Table II Biodistribution of Nanoparticles in Mice at 24 h PI *via* i.v.

%ID/g	Den-PEG	Den-Angio1	Den-Angio4	Den-Angio8
Blood	0.25 ± 0.02	0.24 ± 0.016	0.29 ± 0.00	0.27 ± 0.01
Heart	0.62 ± 0.07	0.56 ± 0.08	0.71 ± 0.06	0.63 ± 0.04
Liver	57.74 ± 5.14	51.85 ± 3.92	56.12 ± 2.79	44.62 ± 8.19
Spleen	15.131 ± 1.42	15.68 ± 0.64	21.54 ± 0.62	17.45 ± 1.27
Lung	4.77 ± 0.42	3.63 ± 1.58	8.40 ± 1.04	8.341 ± 3.65
Kidney	16.49 ± 2.13	15.42 ± 4.60	15.66 ± 1.53	8.90 ± 4.43
Muscle	0.24 ± 0.03	0.16 ± 0.02	0.26 ± 0.05	0.16 ± 0.03
Brain	0.0123 ± 0.001	0.023 ± 0.003	0.043 ± 0.001	0.017 ± 0.005

Data were presented as mean ± SD, (n = 4)

molecules attracted by the hydrophilic peptides may shield the charge of the nanoparticles. Furthermore, the polydispersity indexes of all the nanoparticles were measured below 0.35, which indicates the molecular weight distribution of the nanoparticles kept in a narrow range even after multiple modification steps. Photospectroscopic studies demonstrated that averagely 1.5 IR783 and 1.0 rhodamine were conjugated on each nanoparticle. ^{1}H NMR studies indicated there were about 1.2, 4.2 and 8.1 angiopep-2 peptides conjugated on Den-Angio1, Den-Angio4 and Den-Angio8 respectively. To evaluate the role of multivalent effect played in enhancing the association between the nanoparticles and LRP receptor, flow cytometry studies were conducted with human glioma U87MG cancer cells expressing LRP receptors (Ref). Notably, the receptor binding affinities of nanoparticles increased with the labeling degree of angiopep2 peptide, and the values of Den-Angio1, Den-Angio4 and Den-Angio8 were measured as 3.8, 6.7 and 7.5 times higher than that of control nanoparticle Den-PEG (Fig. S2). Above studies indicate that the multivalent effect can significantly increase the binding affinities between the nanoparticles and LRP receptor.

Biodistribution Studies

To clarify the multivalent effect to the intracerebral uptake of the nanoparticles, biodistribution were investigated in CRI mice at 2 and 24 h post-injection (PI) of the nanoparticles labeled with radioactive ^{125}I (Tables II and S1). All nanoparticles demonstrated their highest concentrations in the liver and the values increased with time after injection. The high expression level of LRP receptors in liver may faciliate the hepatic uptake of the nanoparticles (29). High concentrations of nanoparticles were also found in spleen and kidney, which implied these nanoparticles were excreted through both urinary and biliary pathways. All nanoparticles labeled with angiopep-2 peptides demonstrated higher cerebral uptakes than the control nanoparticle. However, the nanoparticle concentrations in brain were not proportional to the labeling degree of peptide but with a sequence of Den-Angio4 > Den-Angio1 > Den-Angio8 > Den-PEG. The cerebral uptake of Den-Angio4 with a value of 0.043 ± 0.003%ID/g was 3.6, 1.9 and 2.5 times higher than that of Den-PEG (0.012 ± 0.001%ID/g), Den-Angio1 (0.023 ± 0.002%ID/g) and Den-Angio8 (0.017 ± 0.003%ID/g) at 24 h PI (Table II and Fig. 3). Compared to Den-Angio1, the higher concentration of Den-Angio4 in brain should contribute to the multivalent effect that may enhance the efficacy of receptor-mediated endocytosis. The relatively low cerebral uptake of Den-Angio8 may attribute to the abnormal reticuloendothelial system (RES) response that accelerates the clearance of nanoparticles from circulation system and increases the hepatic and splenic uptakes. Above experimental results indicated that ligand density

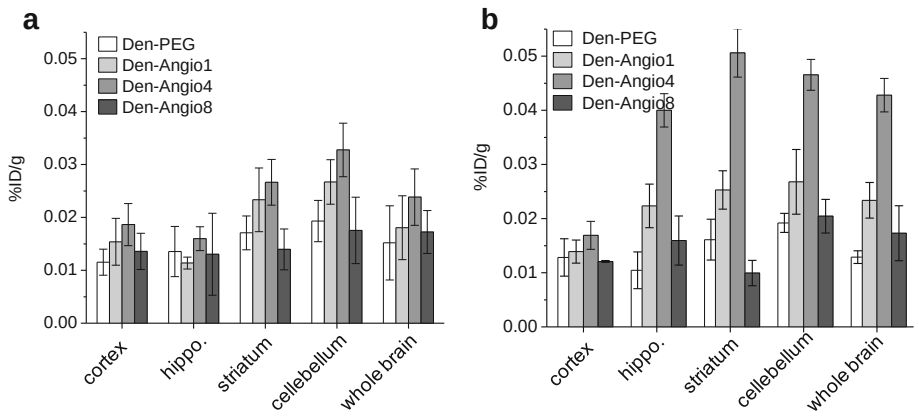

Fig. 3 Biodistribution of ^{125}I labeled nanoparticles (3.7×10^5 Bq/mouse) in brain of healthy mice ($n = 4$) at 2 (**a**) 24 h (**b**) PI *via* i.v.. Columns present mean values, and bars present the data range (SD).

Table III Intracerebral Biodistribution of Nanoparticles at 24 h PI

%ID/g	Den-PEG	Den-Angio1	Den-Angio4	Den-Angio8
Cerebral cortex	0.015 ± 0.003	0.013 ± 0.002	0.017 ± 0.003	0.013 ± 0.000
Hippocampus	0.010 ± 0.003	0.022 ± 0.010	0.040 ± 0.016	0.016 ± 0.007
Striatum	0.014 ± 0.004	0.031 ± 0.000	0.051 ± 0.008	0.010 ± 0.002
Cerebellum	0.017 ± 0.002	0.027 ± 0.009	0.047 ± 0.005	0.020 ± 0.010

Data were presented as mean ± SD, (n = 4)

optimization on nanoparticle is prerequisite to maximize the multivalent effect associated cerebral uptake. Unexpectedly, the intracerebral delivery of the control nanoparticle Den-PEG was indeed observed even its concentration was significantly lower than other nanoparticles. We suspect that Den-PEG may traverse BBB *via* adsorptive-mediated endocytosis that is initiated by the affiliation between the positive charged nanoparticle and the negative charged surface of the brain capillary endothelial cells (BCECs) (30,31). Additionally, a hetergeneous distribution of the nanoparticles in the brain sub-regions was observed (Tables III and S2). The nanoparticle concentrations in hippocampus, striatum and cerebellum were obviously higher than that in the cerebral cortex. For example, the uptake of Den-Angio4 in hippocampus, striatum and cerebellum were measured 0.040 ± 0.003%ID/g, 0.051 ± 0.005%ID/g and 0.047 ± 0.004%ID/g, which were 2.4, 3.0 and 2.8 times higher than that of cerebral cortex (0.017 ± 0.001%ID/g) at 24 h PI (Fig. 3).

Autoradiographic Studies

Autoradiographic images displayed the intracerebral distribution of the nanoparticles at 2 and 24 h PI (Fig. 4). Generally, the nanoparticles first entered cerebellum and then observed in the hippocampus and striatum. In contrast, only trace amount of nanoparticle was detected in the cerebral cortex. Den-Angio4 demonstrated the highest cerebral uptakes in all nanoparticles. Previous studies demonstrated the similar LRP expression levels in cerebellum, hippocampus and cerebral cortex (29), which is hardly to explain the heterogeneous uptake of the nanoparticle in brain subregions. Recent reports clarified that the nanoparticle uptake efficacy in brain sub-regions not only correlates with the expression level of LRP receptors, but also depends on the local concentration of endogenous LRP receptor inhibitors such as receptor-associated protein (RAP) (32). Therefore, the heterogeneous distribution of nanoparticle in the brain could be resulted from the uneven interplay between the LRP receptor and its inhibitors.

Optical Imaging Studies

BBB permeability of the nanoparticles was further verified by the *in vivo* NIR fluorescence imaging (Fig. 5a). The optical image of an enlarged mouse head clearly indicated the

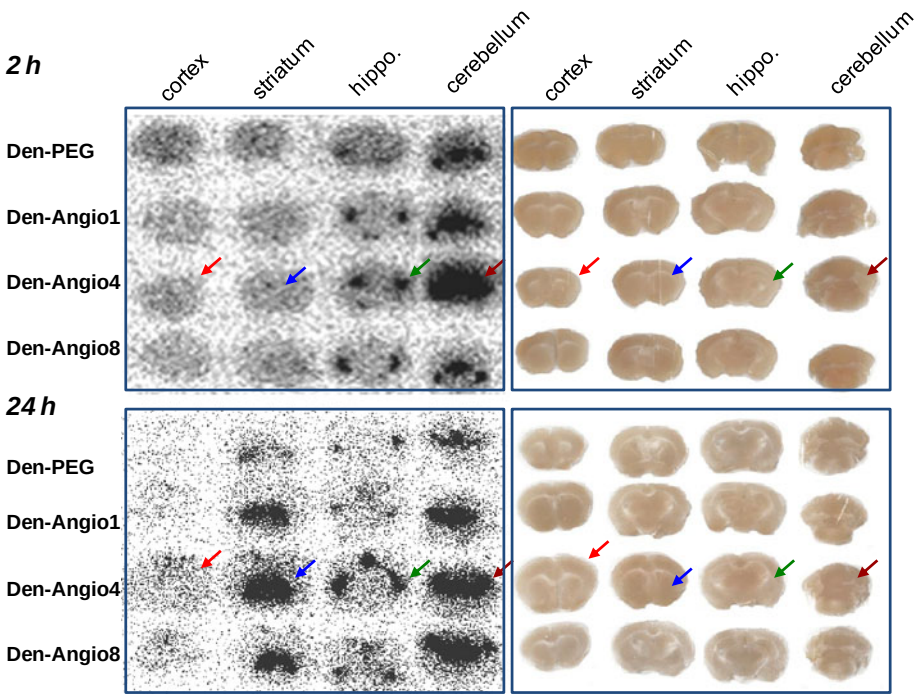

Fig. 4 Representative autoradiographic images and corresponding white-light microscopic images of mouse brain sections at 2 and 24 h PI of the ^{125}I radiolabeled nanoparticle. Brain sections were chosen to best present the cortex, striatum, hippocampus and cerebellum areas. Arrows point to the cortex (*red*), striatum (*blue*), hippocampus (*green*) and cerebellum (*brown*) of a brain at 2 and 24 h PI of Den-Angio4 (3.7×10^5 Bq/mouse).

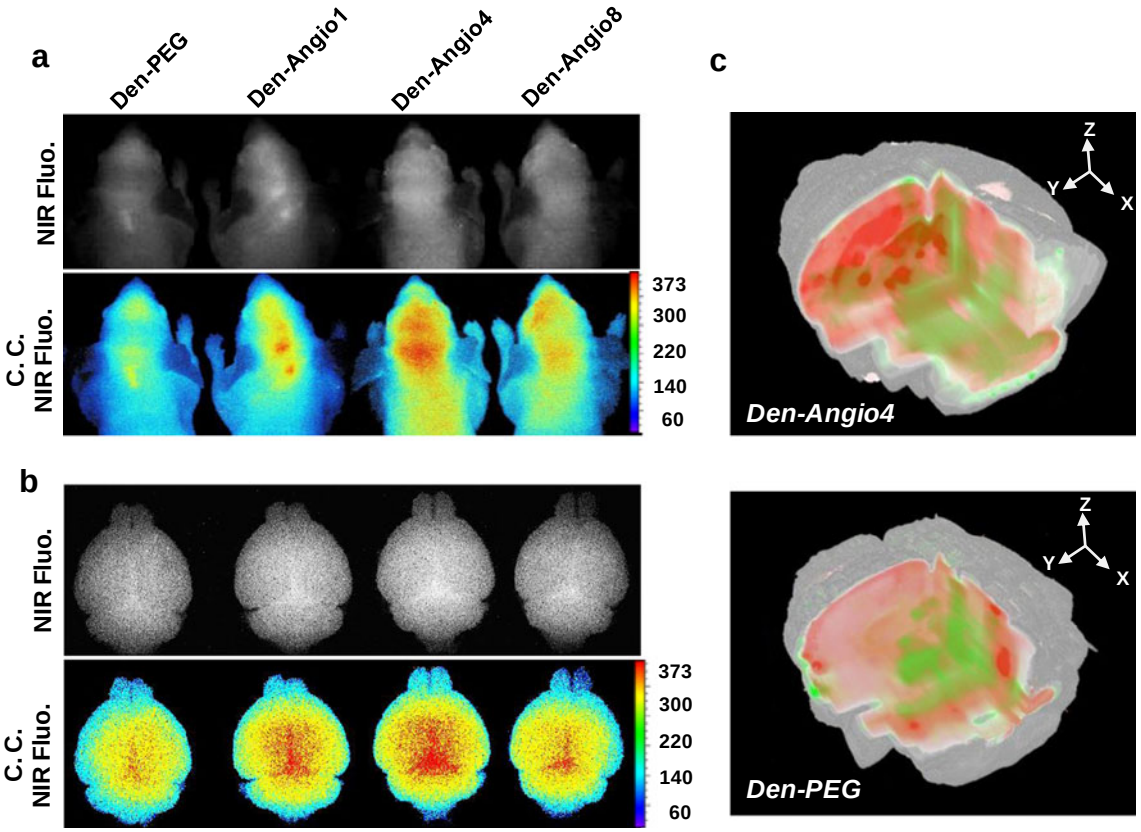

Fig. 5 NIR fluorescence imaging demonstrated the highest BBB permeable efficacy of Den-Angio4. (**a**) *In vivo* NIR fluorescence and color coded (c. c.) fluorescence images of mouse brain area at 24 h PI of nanoparticle (5.0 nmol/mouse). (**b**) *Ex vivo* NIR fluorescence images of excised whole brains at 24 h PI of nanoparticle. **c** Representative triplanar views of 3D reconstructed NIR fluorescence images of mouse brain at 24 h PI of Den-PEG or Den-Angio4 with a same dose (5.0 nmol/mouse) *via* i.v. NIR fluorescence presenting the nanoparticle was displayed in *red* and DiO fluorescence presenting vasculatures was displayed in *green*.

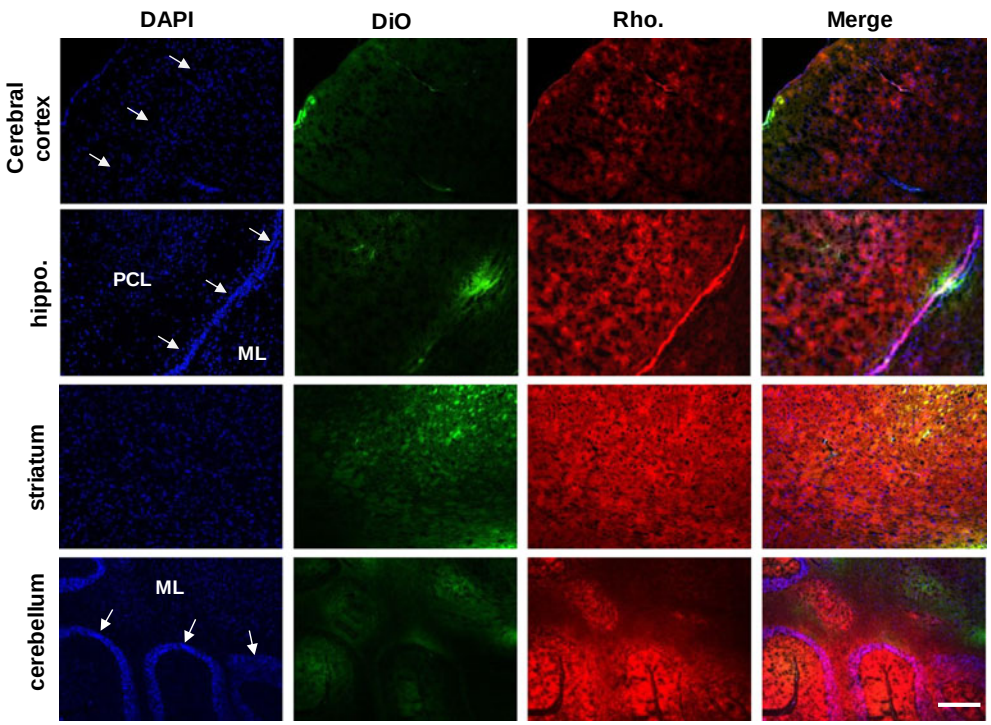

Fig. 6 Den-Angio4 demonstrated the heterogeneous distribution in sub-brain areas after penetrating BBB. Representative fluorescence microscopic images of the cortex, striatum, hippocampus and cerebellum areas at 24 h PI of Den-Angio4 (5 nmol/mouse) *via* i.v.. The nuclear stainned by DAPI was displayed in *blue*, vasculatures stainned by DiO was displayed in *green*, the rhodamine fluorescence of nanoparticle was displayed in *red*. The colocalization between rhodamine and DiO fluorescence is indicated by the *yellow color* in the merged images. *Arrows* indicate the granular cell layer in the cerebral cortex, hippocampus and cerebellum. Bar: 100 μm. *PCL* pyramidal cell layer; *ML* molecular layer.

cerebral uptakes of all nanoparticles at 24 h PI *via* i.v.. Correlated well with the biodistribution results, the average NIR fluorescence on the mouse brain area was quantified with an order of Den-Angio4 > Den-Angio1 > Den-Angio8 > Den-PEG. The fluorescence of Den-Angio4 was determined as 2.6 times higher compared to that of Den-PEG (Fig. S2a). *Ex vivo* NIR fluorescence images of the excised whole brains indicated that the average fluorescence intensity of Den-Angio4 was 1.9 times higher compared to that of Den-PEG (Fig. 5b, Fig. S2B). To straightforwardly visualize the intracerebral distribution of the nanoparticles, three dimensional (3D) NIR fluorescence images of the brains were reconstructured at 24 h PI of Den-Angio4 or Den-PEG (Fig. 5c). The vasculatures were stained by a lipophilic fluorescence dye: 3,3′-dioctadecyloxacarbocyanine perchlorate (DiO) to highlight the spatial correlation between the vasculature density and the nanoparticle concentration. In contrast to the non-specifically distributed Den-PEG in the brain, the fluorescence signal of Den-Angio4 as "hot spots" was distributed in hippocampus, striatum and cerebellum at 24 h PI. The abundant vasculatures such as posterior cerebral artery, longitudinal hippocampal vein *et al.* in above regions may strenghthen the nanoparticle delivery. The co-registeration between the fluorescence of nanoparticle and vasculature supports above assumption.

Fluorescence Microscopic Imaging Studies

Figure 6 shows the representative fluorescence microscopic images of brain sub-regions at 24 h PI of Den-Angio4. The fluorescence intensities of Den-Angio4 in hippocampus, striatum and cerebellum were obviously higher than that in cerebral cortex. In the hippocampus, with the reference of the cell nuclei that were stainned by DAPI, the nanoparticle mainly distributed in the granule cell layer and pyramidal cell layer but rarely in the outward molecular cell layer. In the cerebellum, the nanoparticle was mainly accumulated in the granule cell layer, but few found in the white matter and molecular layer. In the striatum, the nanoparticle as vesicular structures accumulated in the medium spiny neurons. Bu *et al.* systemically investigated the intracerebral distribution of LRP receptor in the mouse brain and found that this receptor is highly expressed in the granule, pyramidal and Purkinje cells, but barely found in the white matter and molecular cell layer that was made up of the stellate cellsand basket cells (14,29). The distribution pattern of Den-Angio4 in the brain indicates that this nanoparticle may first traverse the BBB *via* receptor-mediated endocytosis and secondly target the neurons with high LRP receptor density.

CONCLUSIONS

In conclusion, we developed a series of nanoparticles that were labeled imaging reporter as well as different numbers of BBB permeable angiopep-2 peptides. *In vitro* flow cytometry studies showed that the multivalent effect significantly increased the binding affinity between the nanoparticle and the cells expressing LRP receptors. Bio-distribution and *in vivo* optical imaging studies demonstrated the multivalent effect up-regulated the intracerebral delivery of the nanoparticle by enhancing the BBB traverse efficacy . Considering the high expression level of LRP receptors in different types of brain cancer cells and the neurons with up-regulated Aβ peptide, Den-Angio4 as a prototype holds promise for diagnosis or treatment of CNS diseases such as brain tumors and Alzheimer's disease without the compromise to BBB.

ACKNOWLEDGMENTS AND DISCLOSURES

Xihui Gao and Jun Qian contributed equally to this work. This work was supported by the National Basic Research Program of China (973 Program, 2013CB733801), the National Natural Science Foundation of China (Nos. 81171384,) and Shenzhen Bio-industry Development Fund Basic Research Program (JC201005280607A).

REFERENCES

1. Hutchinson E. Blood–brain barrier: plugging the leak. Nat Rev Neurosci. 2010;11:789.
2. Pardridge WM. Blood–brain barrier delivery. Drug Discov Today. 2007;12:54–61.
3. Fishman JB, Rubin JB, Handrahan JV, Connor JR, Fine RE. Receptor-mediated transcytosis of transferrin across the blood–brain barrier. J Neurosci Res. 1987;18:299–304.
4. Gabathuler R. Approaches to transport therapeutic drugs across the blood–brain barrier to treat brain diseases. Neurobiol Dis. 2010;37:48–57.
5. Zhang P, Hu L, Yin Q, Zhang Z, Feng L, Li Y. Transferrin-conjugated polyphosphoester hybrid micelle loading paclitaxel for brain-targeting delivery: synthesis, preparation and *in vivo* evaluation. J Control Release. 2012;159:429–34.
6. Ulbrich K, Hekmatara T, Herbert E, Kreuter J. Transferrin- and transferrin-receptor-antibody-modified nanoparticles enable drug delivery across the blood–brain barrier (BBB). Eur J Pharm Biopharm 2009;71:251–6.
7. Huang RQ, Qu YH, Ke WL, Zhu JH, Pei YY, Jiang C. Efficient gene delivery targeted to the brain using a transferrin-conjugated polyethyleneglycol-modified polyamidoamine dendrimer. FASEB J Off Publ Fed Am Soc Exp Biol. 2007;21:1117–25.
8. Visser CC, Voorwinden LH, Crommelin DJ, Danhof M, de Boer AG. Characterization and modulation of the transferrin receptor on brain capillary endothelial cells. Pharm Res. 2004;21:761–9.
9. Zhan C, Li B, Hu L, Wei X, Feng L, Fu W, *et al.* Micelle-based brain-targeted drug delivery enabled by a nicotine acetylcholine receptor ligand. Angew Chem Int Ed Engl. 2011;50:5482–5.

10. Demeule M, Regina A, Che C, Poirier J, Nguyen T, Gabathuler R, *et al.* Identification and design of peptides as a new drug delivery system for the brain. J Pharmacol Exp Ther. 2008;324:1064–72.
11. Liu Y, Huang R, Han L, Ke W, Shao K, Ye L, *et al.* Brain-targeting gene delivery and cellular internalization mechanisms for modified rabies virus glycoprotein RVG29 nanoparticles. Biomaterials. 2009;30:4195–202.
12. Huang R, Ke W, Liu Y, Jiang C, Pei Y. The use of lactoferrin as a ligand for targeting the polyamidoamine-based gene delivery system to the brain. Biomaterials. 2008;29:238–46.
13. Yan H, Wang L, Wang J, Weng X, Lei H, Wang X, *et al.* Two-order targeted brain tumor imaging by using an optical/paramagnetic nanoprobe across the blood brain barrier. ACS Nano. 2012;6:410–20.
14. Lillis AP, Van Duyn LB, Murphy-Ullrich JE, Strickland DK. LDL receptor-related protein 1: unique tissue-specific functions revealed by selective gene knockout studies. Physiol Rev. 2008;88:887–918.
15. Ulery PG, Beers J, Mikhailenko I, Tanzi RE, Rebeck GW, Hyman BT, *et al.* Modulation of beta-amyloid precursor protein processing by the low density lipoprotein receptor-related protein (LRP). Evidence that LRP contributes to the pathogenesis of Alzheimer's disease. J Biol Chem. 2000;275:7410–5.
16. Liu S. Radiolabeled multimeric cyclic RGD peptides as integrin alphavbeta3 targeted radiotracers for tumor imaging. Mol Pharm. 2006;3:472–87.
17. Chakraborty S, Shi J, Kim YS, Zhou Y, Jia B, Wang F, *et al.* Evaluation of 111In-labeled cyclic RGD peptides: tetrameric not tetravalent. Bioconjug Chem. 2010;21:969–78.
18. Barrett T, Ravizzini G, Choyke PL, Kobayashi H. Dendrimers in medical nanotechnology. IEEE Eng Med Biol Mag Q Mag Eng Med Biol Soc. 2009;28:12–22.
19. Gilliesand ER, Frechet JM. Dendrimers and dendritic polymers in drug delivery. Drug Discov Today. 2005;10:35–43.
20. Whitesides GM. The 'right' size in nanobiotechnology. Nat Biotechnol. 2003;21:1161–5.
21. Hong S, Leroueil PR, Majoros IJ, Orr BG, Baker Jr JR, Banaszak Holl MM. The binding avidity of a nanoparticle-based multivalent targeted drug delivery platform. Chem Biol. 2007;14:107–15.
22. Achilefu S. Rapid response activatable molecular probes for intraoperative optical image-guided tumor resection. Hepatology. 2012;56:1170–3.
23. Weisslederand R, Ntziachristos V. Shedding light onto live molecular targets. Nat Med. 2003;9:123–8.
24. Yan H, Wang J, Yi P, Lei H, Zhan C, Xie C, *et al.* Imaging brain tumor by dendrimer-based optical/paramagnetic nanoprobe across the blood–brain barrier. Chem Commun (Camb). 2011;47(8130–8132).
25. Li C, Winnard Jr P, Bhujwalla ZM. Facile synthesis of 1-(acetic acid)-4,7,10-tris(tert-butoxycarbonylmethyl)-1,4,7,10-tetraazacyclododecane: a reactive precursor chelating agent. Tetrahedron Lett. 2009;50:2929–31.
26. Boltonand AE, Hunter WM. The labelling of proteins to high specific radioactivities by conjugation to a 125I-containing acylating agent. Biochem J. 1973;133:529–39.
27. Hilderbrand SA, Kelly KA, Weissleder R, Tung CH. Monofunctional near-infrared fluorochromes for imaging applications. Bioconjug Chem. 2005;16:1275–81.
28. Li C, Greenwood TR, Bhujwalla ZM, Glunde K. Synthesis and characterization of glucosamine-bound near-infrared probes for optical imaging. Org Lett. 2006;8:3623–6.
29. Bu G, Maksymovitch EA, Nerbonne JM, Schwartz AL. Expression and function of the low density lipoprotein receptor-related protein (LRP) in mammalian central neurons. J Biol Chem. 1994;269:18521–8.
30. Lu W, Sun Q, Wan J, She Z, Jiang XG. Cationic albumin-conjugated pegylated nanoparticles allow gene delivery into brain tumors *via* intravenous administration. Cancer Res. 2006;66:11878–87.
31. van Rooy I, Cakir-Tascioglu S, Hennink WE, Storm G, Schiffelers RM, Mastrobattista E. *In vivo* methods to study uptake of nanoparticles into the brain. Pharm Res. 2011;28:456–71.
32. Suzuki Y, Nagai N, Yamakawa K, Kawakami J, Lijnen HR, Umemura K. Tissue-type plasminogen activator (t-PA) induces stromelysin-1 (MMP-3) in endothelial cells through activation of lipoprotein receptor-related protein. Blood. 2009;114:3352–8.